A novel method to evaluate gamma camera rotational uniformity and sensitivity variation

S. Cheenu Kappadath,[a] William D. Erwin, and Richard E. Wendt III
Department of Imaging Physics, The University of Texas MD Anderson Cancer Center, Houston, Texas 77030

(Received 10 October 2008; revised 7 April 2009; accepted for publication 8 April 2009; published 5 May 2009)

An alternative to the conventional method of performing the AAPM Report 52 rotational uniformity and sensitivity test has been developed. In contrast to the conventional method in which a Co-57 sheet source is fastened to the collimator, this new point-source method acquires the images intrinsically using a Tc-99m point source placed near the isocenter of gantry rotation. As with the conventional method, the point-source method acquires 5×10^6 count flood images at four distinct gantry positions to calculate the maximum sensitivity variation (MSV)—a quantitative metric of rotational uniformity and sensitivity variation. The point-source method incorporates corrections for the decay of Tc-99m between acquisitions, the curvature in the image intensity due to variation in photon flux across the detector from a near-field source, and the source-to-detector distance variations between views. The raw point-source images were fitted with an analytic function in order to compute curvature- and distance-corrected images prior to analysis. Five independent MSV measurements were performed using both conventional and point-source methods on a single detector of a dual-headed SPECT system to estimate the precision of each method. The precision of the point-source method was further investigated by performing ten independent measurements of MSV on six different detectors. Correlation between the MSV calculated by the two methods was investigated by performing the test on nine different detectors using both methods. Different levels of sensitivity variations were also simulated on four detectors to generate 40 additional paired points for correlation analysis. The effect of the total image counts on the MSV estimated with the new method was evaluated by acquiring image sequences with 5×10^6, 10×10^6, and 20×10^6 count images. The MSV calculated using the conventional and point-source methods exhibited a high degree of correlation and consistency with equivalence. The precision of the point-source method (0.145%) is lower than the conventional method (0.04%) but sufficient to test MSV. No statistically significant dependence of MSV with the point-source method on the total image counts over a range of $(5-20)\times10^6$ counts was observed. Curvature correction of the images prior to the generation of difference images renders images more conducive to qualitative inspection for structured, nonrandom patterns. The advantages of the new methodology are that multiple detectors of a gamma camera can be evaluated simultaneously which substantially reduces the time required for MSV testing and the reduced risk of accidental damage to the collimators and patient proximity detection system from having to mount a sheet source on each of the detectors. [DOI: 10.1118/1.3125642]

Key words: gamma camera, rotational uniformity, curvature correction, point source

I. INTRODUCTION

The use of single-photon emission computed tomography (SPECT) has become widespread since its introduction in the late 1970s. High-quality and artifact-free SPECT imaging requires routine performance of quality control procedures. Acceptance and quality control tests of SPECT systems have been previously described in the NEMA Standard NU 1-1994 and AAPM Reports 22 and 52.[1–3] One important test involves an evaluation of the rotational uniformity and sensitivity variation of the SPECT system, because artifact-free SPECT images require essentially identical uniform and sensitive detector response at all angular views.

One of the main reasons for rotational variability in uniformity and sensitivity arises from the fact that the photomultiplier tubes (PMTs) present in the gamma camera detectors exhibit gain variations when their spatial orientations change with respect to an external magnetic field.[4] Due to the use of Anger logic for spatial localization, shifts in PMT gain could introduce shifts in the calculation of the photon energy and interaction location. Such effects can be produced by the Earth's magnetic field or local magnetic fields present in the SPECT scanner room. Local magnetic fields could also arise from the presence of a nearby cyclotron or MRI system or if the room had been previously exposed to high magnetic field strengths such that the structural steel might have been magnetized. Such situations are becoming increasingly common, since space in modern clinics is usually scarce and scanner rooms are periodically remodeled for reuse. Historically,

manufacturers have incorporated magnetic shielding into SPECT detector assemblies to minimize such PMT gain shifts (e.g., wrapping PMTs in μ metal). Other sources of image nonuniformity due to gantry rotation include thermal gradients within the detector housing and gravitational-mechanical effects.[5]

The conventional procedure to evaluate rotational uniformity and sensitivity variation of the SPECT system has been described in AAPM Report 52 and NEMA NU 1-1994. A synopsis of the procedure is to mechanically secure a Co-57 sheet source to the detector assembly with collimation and collect a 5×10^6 count, 64×64 pixel image with the detector first at the 0° (or 12 o'clock) position or orientation and record the acquisition time T. The image acquisition is repeated for time T with the detector at the 90° (3 o'clock), 180° (6 o'clock), 270° (9 o'clock), and 360° (12 o'clock) positions. The total counts in each of the images at the 90°, 180°, 270°, and 360° positions are calculated and the maximum ($C_{\max}$) and minimum ($C_{\min}$) counts among them is determined. The maximum sensitivity variation (MSV), a quantitative metric, is calculated as[3]

$$\mathrm{MSV}(\%) = (C_{\max} - C_{\min})/(C_{\max} + C_{\min}) \times 100.$$

AAPM Report 52 recommends an acceptable camera performance criterion for MSV of 0.75% or less. For visual inspection, the 0° image is subtracted from the 90°, 180°, 270°, and 360° images, and the 90° image is subtracted from the 270° image. The difference images are then evaluated qualitatively for structured, nonrandom patterns. This completes the evaluation of one detector. The entire test procedure and analysis are repeated for the second (or third) detector if one is evaluating a multiple detector SPECT system.

One of the major drawbacks of the AAPM method is that only a single detector can be evaluated at a time. This leads to long test times of 1.5–2 h for a modern dual-headed gamma camera system. The other major drawback is that the AAPM procedure is somewhat cumbersome and involves risk of damage to the collimator and patient proximity sensor while one mounts the source, rotates the gantry, and unmounts the source on each of the gamma camera detectors during testing.

In this work, a new methodology for evaluation of rotational uniformity and sensitivity variation for SPECT systems is proposed. The new (point-source) method acquires the required images concurrently on all detectors without collimation using a Tc-99m point source located near the isocenter. An analytic function has been derived to describe the curvature in the signal intensity of the point-source image including decay and distance corrections. Correlations between the MSV calculated by the two methods were investigated. The precision of MSV measurements for each of the methods was calculated. The effect of the total image count on the MSV was also investigated. A qualitative evaluation of difference images for structured, nonrandom patterns without and with curvature correction was also performed.

II. MATERIALS AND METHODS

The proposed point-source methodology for the rotational uniformity and sensitivity variation test acquires the required images at the 0°, 90°, 180°, 270°, and 360° gantry positions intrinsically (i.e., without collimation) using a Tc-99m point source ($\sim5\times5\times5$ mm^3 cotton ball) of about 90 kBq (~25 μCi) placed near the isocenter of the SPECT gantry. As in the conventional method, the image acquisitions with the detector at the 90°, 180°, 270°, and 360° gantry positions were for the same duration as the time required for the 5×10^6 count 64×64 image with the detector at 0°.

A major advantage of the point-source method is that images from all (usually two) detectors of a SPECT system can be acquired concurrently, which substantially reduces the total acquisition time. Nonetheless, there are three concerns to be addressed prior to MSV calculation using the point-source methodology: (1) Decay of Tc-99m between image acquisitions at the different positions, (2) image curvature due to inverse-square ($1/R^2$) variation in photon flux across the detector from a near-field point source and the effective thickness of the crystal at oblique angles of incidence, and (3) source-to-detector distance variation between the different gantry positions since the Tc-99m point source is placed only approximately at the isocenter.

Compensation for the decay of Tc-99m between different image acquisitions, which leads to loss of image counts, was performed by calculating the differences between the first and each subsequent image start time and normalizing the image counts to the time of the 0° image (t_0). The start time of each image acquisition (t_i) was extracted from the DICOM header, and the pixel values (counts) in each image were decay corrected to the time of the first image (t_0) using the scale factor $e^{\ln 2\times(t_i-t_0)/T_{1/2}}$, where $T_{1/2}$ represents the half-life of Tc-99m (6.017 h).

The remediation of the other two concerns began by first constructing a mathematical model for the point-source photon flux as measured by the detector, that takes into consideration the inverse-square ($1/R^2$) variation in photon flux across the detector from a near-field point source, the distance of the source from the face of the detector, and the effective thickness of the crystal at oblique angles of incidence. The Appendix describes the derivation of the point-source photon flux f (x_0, y_0, D, N, T) for a point source at a distance D from a detector face, with a crystal thickness T, that projects onto the detector plane at location (x_0, y_0), and N is the normalization scalar related to the source activity.

To correct for image curvature the raw 64×64 pixel images were first masked using a centrally located 50×40 image matrix that defined the useful field of view (or pixels containing image data). A nonlinear least-squares fit of the central 50×40 pixels from each image to the analytic function f was then performed. After the fit, the raw images were multiplied by the curvature-correction image ($1/f$) to yield a flat-field image, where the pixel with the largest count in the fitted point-source image f maintained its value in the curvature-corrected image. To account for small variations in distance between the point source and detector, a distance-

correction term, $(D/D_0)^2$, was applied to normalize the curvature-corrected image to a common distance for all images, where D is the distance computed from the fit. The common distance D_0 was chosen to be 38 cm since the maximum radius for SPECT rotation was ~38 cm for the SPECT systems at our institution.

II.A. Accuracy of source-to-detector distance estimate from the point-source image model

Images of a Tc-99m point source were acquired with two different detectors at four different source-to-detector distances (nominal distances $D=20$, 25, 30, and 35 cm). The true distances from the point source to the detector face were recorded. The point-source images were fitted to the point-source image model (Appendix) to estimate the source-to-detector distances. The mean, standard deviation (SD), and range of difference values between the true source-to-detector distance and those estimated from the fit were calculated. The estimated source-to-detector distances were fitted to a linear model to test for equivalency between estimated and measured values.

II.B. Precision of the MSV calculations

Five independent MSV measurements were performed using both conventional and point-source methods on a single detector of a dual-headed SPECT system. The standard deviations of the five measurements were used to estimate the precision of the MSV calculations for each of the two methods. The experimental setup was completely dismantled before each subsequent run to get a precision estimate that included both statistical fluctuations and setup variability. A two-tailed F test[6] was used to test the null hypothesis of equal variances in the two measurement populations. As discussed in Sec. IV B, the precision of MSV for the conventional method can be derived from error propagation. To get a better estimate of the precision with the point-source method, ten MSV measurements were performed on each of six different [four 9.5 mm (3/8 in.) and two 15.9 mm (5/8 in.) crystal] detectors. The mean of the six variances was used to estimate the precision with the point-source method.

II.C. Correlation between the MSV calculated with the two methods

The MSV was calculated using measured data from nine different detectors using both conventional and point-source methods. Due to the low number of paired points in the measured data for the correlation analysis, different levels of sensitivity variation were also simulated on four detectors to generate 40 additional MSV calculations. The simulation of different sensitivity variations involved scaling the acquired image data for one of the views with 0.9, 0.95, 0.98, 0.99, 0.995, 0.999, 1.05, and 1.1 prior to the recalculation of MSV. Two of the four detectors had additional simulations where image data were scaled with 1.001, 1.005, 1.01, and 1.02. The scaling of the image data was performed on images from both conventional and point-source methods and the MSV using identical scale factors on the same detector were then paired together for the correlation analysis. Agreements in the MSV calculated with two methods were assessed separately for the measured data (9 paired points) and the measured plus simulated data (49 paired points). The Spearman rank correlation coefficient[7] between the two estimates was computed to elucidate correlation between MSV calculations using the two methods. A Bland-Altman plot[8] was generated and analyzed to evaluate bias and confidence in the point-source method relative to the conventional method.

II.D. Dependence of MSV calculation on total image counts for the point-source method

AAPM Report 52 suggests a total image count of 5×10^6 for calculation of the MSV. The impact of total image counts on the MSV estimated with the point-source methodology was evaluated by acquiring the required image sequences with 5×10^6, 10×10^6, and 20×10^6 count images and comparing their respective MSV calculations. The significance of MSV difference when using 5×10^6, 10×10^6, and 20×10^6 count images was statistically evaluated using a Z test.[9] This experiment was performed on two different detectors.

III. RESULTS

III.A. Accuracy of source-to-detector distance estimate from the point-source image model

The source-to-detector distances computed using the fit to the point-source images were found to be slightly greater than the true distances. The mean and standard deviation of difference values between the true source-to-detector distance and those estimated from the fit were 1.4 and 0.3 cm, respectively. The difference values ranged from 1.0 to 1.8 cm. The true source-to-detector distances are plotted against the distances computed using the point-source model fit in

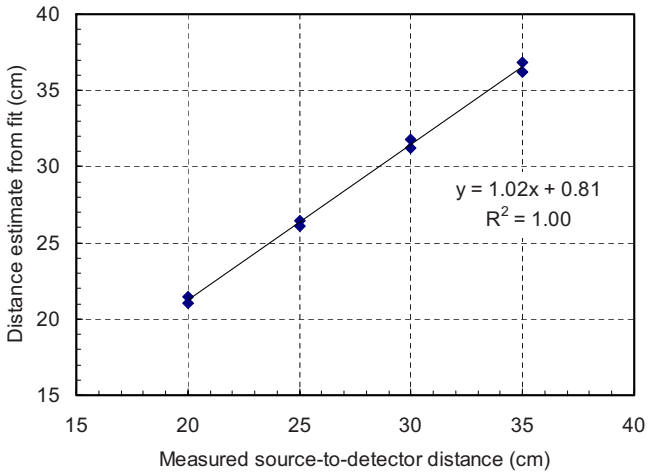

FIG. 1. The source-to-detector distances estimated from the curvature-correction fit to the point-source image plotted against the true distances at four different distances for two different detectors.

TABLE I. The five separate and independent measurements of the maximum sensitivity variation (MSV%) for the same detector using both point-source and the conventional methods together with their mean values, SD, and coefficient of variation (COV).

Method	Point source	Conventional
Sample 1	0.58	0.12
Sample 2	0.49	0.08
Sample 3	0.30	0.13
Sample 4	0.79	0.18
Sample 5	0.36	0.07
Mean	0.50	0.12
SD	0.19	0.04
COV	0.38	0.38

Fig. 1. A least-squares fit of the data to a straight line yielded a slope of 1.02 ± 0.02 and a constant of 0.81 ± 0.51 cm.

III.B. Precision of the MSV calculations

The five separate and independent measurements of MSV using both conventional and point-source methods on a single detector of a dual-headed SPECT system are shown in Table I. The mean MSVs for conventional and point-source methods were computed to be 0.12 and 0.50, respectively, with similar coefficients of variation for the two methods (38%). The precision (σ) of the conventional and point-source methods were measured to be 0.04 and 0.19, respectively.

The ten measurements of MSV for six different detectors [A–D: 9.5 mm (3/8 in.) crystal; E–F: 15.9 mm (5/8 in.) crystals] using the point-source method are shown in Table II. The MSV values for all 60 measurements ranged from a minimum of 0.15 to a maximum of 0.91. The coefficients of variation ranged from 21% to 42% and the measured variance ranged from 0.01 to 0.03. The square root of the mean variance for six detectors was considered to be the precision for the point-source method (=0.145%). The precision of the conventional method (σ=0.04%) was found to be statistically superior to that of the point-source method (σ =0.145%), since the two-tailed F test rejected the null hypothesis of equal variances in the two populations at >98% confidence level ($p<0.02$).

III.C. Correlation between the MSV calculated with the two methods

The MSV calculated using conventional and point-source methods for the nine detectors are plotted in Fig. 2(a) with error bars corresponding to the precision values calculated for each method from Sec. III B. A perfect agreement between the two methods for the nine detectors was not observed since the data do not lie along the line of equality. In addition, there appeared to be no obvious correlation, linear or otherwise, between MSV calculated with the two methods. The Spearman rank correlation coefficient between the two estimates was 0.10, which is statistically consistent with no correlation ($p>0.50$) between them.

The simulated MSV calculations using conventional and point-source methods for the measured data combined with simulated data are shown in Fig. 2(b). The cluster of points near ~2.5 and ~5 correspond to simulated sensitivity variation scale factors of 0.95 or 1.05 and 0.9 or 1.1, respectively. A high degree of correlation was observed between the two methods as shown in Fig. 2(b). The Spearman rank correlation coefficient between the two estimates was 0.93, which is consistent with a (linear) correlation with >99.99% confidence level. In addition, a least-squares fit of a straight line to the data yielded a constant of 0.15 ± 0.04 and slope of 0.981 ± 0.015. The deviation of the fitted slope value from unity was not statistically significant (<95% confidence level). In fact, a straight line with slope unity was also

TABLE II. The ten measurements of the maximum sensitivity variation (MSV%) for six different detectors [A–D: 9.5 mm (3/8 in.) crystal; E–F: 15.9 mm (5/8 in.) crystals] using the point-source method together with their mean values, SD, COV, variance, minimum, and maximum values.

Detector	A	B	C	D	E	F
Sample 1	0.50	0.33	0.48	0.71	0.39	0.51
Sample 2	0.90	0.49	0.19	0.43	0.64	0.75
Sample 3	0.59	0.44	0.18	0.29	0.56	0.33
Sample 4	0.80	0.28	0.46	0.34	0.26	0.21
Sample 5	0.48	0.33	0.28	0.40	0.36	0.48
Sample 6	0.43	0.33	0.32	0.19	0.36	0.48
Sample 7	0.69	0.40	0.36	0.38	0.15	0.48
Sample 8	0.91	0.49	0.31	0.59	0.62	0.37
Sample 9	0.57	0.30	0.56	0.49	0.49	0.56
Sample 10	0.52	0.35	0.44	0.51	0.22	0.50
Mean	0.64	0.37	0.36	0.43	0.40	0.47
SD	0.18	0.08	0.13	0.15	0.17	0.14
COV	0.28	0.21	0.36	0.35	0.42	0.31
Variance	0.03	0.01	0.02	0.02	0.03	0.02
Maximum	0.91	0.49	0.56	0.71	0.64	0.75
Minimum	0.43	0.28	0.18	0.19	0.15	0.21

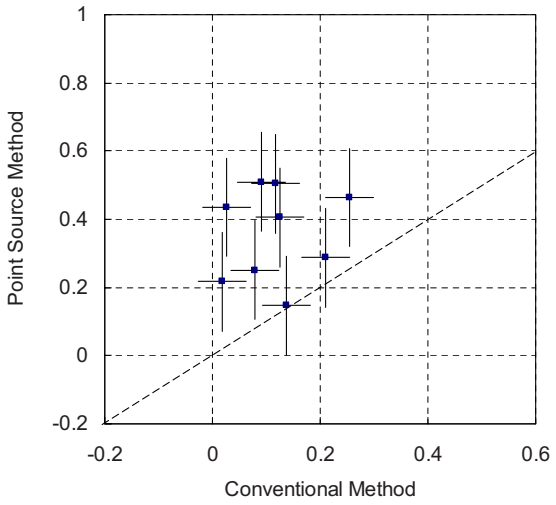

(a)

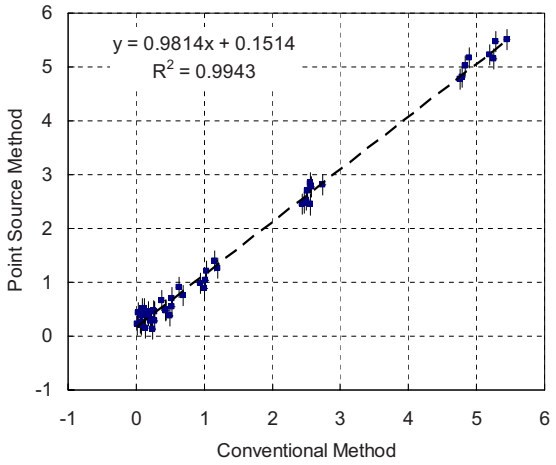

(b)

FIG. 2. The maximum sensitivity variation calculated with the point-source method plotted against that for the conventional method. The error bars shown are the precision estimates for each of the two methods (Sec. III C and Table I). (a) Paired points for the measured data from nine different detectors. The dashed line plotted is the line of equality with slope of unity and intercept of zero. (b) Paired points for the measured data combined with simulated data. The dashed line plotted is the fit of the data to a straight line.

deemed to be an acceptable description of the data (reduced chi-squared value of 0.52) that yielded a constant value of 0.12 ± 0.03. Therefore, inclusion of simulated data suggested good agreement of MSV between the conventional and point-source methods.

Figure 3 shows the Bland-Altman plot for the MSV calculation using the two methods for the measured data combined with the simulated data, with the mean of the two measurements as the abscissa and the difference between them as the ordinate. The difference in MSV did not trend with the average MSV. The mean and standard deviation of the differences are 0.12% and 0.14%, respectively. The mean difference could be interpreted as an estimate of the bias for MSV calculations with the point-source method. With a standard error ($\equiv\sqrt{\sigma^2/n}$) in the mean difference of 0.02% and 48 degrees of freedom, the 95% confidence interval for the bias is 0.08%–0.16%.

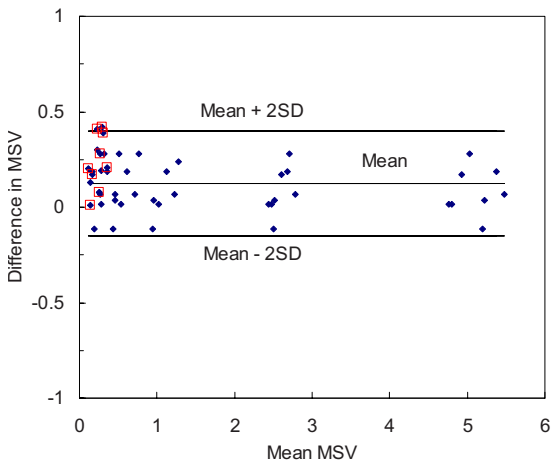

FIG. 3. A Bland-Altman plot of agreement in MSV calculated with both point-source and conventional methods. The graph plots the mean of the two measurements as the abscissa and the difference between them (point-source minus conventional) as the ordinate. The data plotted include MSV for the nine detectors (identified by square boxes) and the simulated data. The mean difference (bias) in the point-source method and the ± 2 SD limits are also indicated.

III.D. Dependence of MSV calculation on total image counts for the point-source method

The MSV calculated with the point-source method by using image sequences with 5×10^6, 10×10^6, and 20×10^6 count images are shown in Table III for two different detectors. For detector A the lowest MSV was calculated for the 10×10^6 count images, whereas for detector B the lowest MSV was calculated for the 5×10^6 count images. The range of MSV with higher image counts was smaller than or similar to the precision of the MSV with 5×10^6 count images. Therefore, a consistent trend was not inferred for the point-source method MSV calculation as a function of the total image count. According to the Z test, a difference in MSV with $>95\%$ confidence will be realized only for MSV differences greater than $1.96\times0.145\% = 0.28\%$, assuming that the precision of 0.145% for MSV measured with a point-source method is independent of the total image counts. The measured range of MSV calculated for total image counts of 5

TABLE III. The maximum sensitivity variation (MSV%) for two different detectors (A and B) with the point-source method using image sequences with 5×10^6, 10×10^6, and 20×10^6 counts per image. The SD and range of MSV calculated are also shown.

Detector	A	B
5×10^6 counts	0.43	0.15
10×10^6 counts	0.24	0.22
20×10^6 counts	0.29	0.21
SD	0.10	0.04
Range	0.19	0.07

$\times 10^6$, 10×10^6, and 20×10^6 counts was 0.07%–0.19% (which is <0.28%). Therefore, a statistically significant dependence of MSV on total image counts over a range of $(5-20)\times 10^6$ counts was not inferred.

IV. DISCUSSION

IV.A. Accuracy of source-to-detector distance estimate from the point-source image model

The point-source image model estimates D as the distance from the point source to the best estimate of the effective image plane. The measured value D reflects the distance from the point source to the surface of the detector assembly. The measured D does not account for the thicknesses of the aluminum cover or the coating of reflective material over the detector face that are part of the hermetic seal for NaI(Tl) crystals. In addition, the mean depth of interaction of about 0.26 cm at 140 keV for NaI crystals suggests that the effective image plane lies that distance below the surface of the crystal. These three factors help explain the larger estimates for D using the point-source image fit compared to the measured D values. Accounting for a difference of 0.26 cm in the least-squares fit of the data (Fig. 1) results in a constant value of 0.55 ± 0.51 cm. Using the Z test, the remaining constant value of 0.55 cm is not statistically significant ($p=0.28$). Therefore, the estimated source-to-detector distance from the fit can be considered to be statistically equivalent to the expected value. The variability in MSV due to the small uncertainty of the source-to-detector distance (~0.5 cm) has been accounted for in the MSV precision measurements for the point-source method (Sec. III B).

IV.B. Precision of the MSV calculations

The one σ statistical uncertainty for MSV, σ_{MSV}, estimated by error propagation yields the expression $\sigma_{\mathrm{MSV}}=1/(\sqrt{2}\cdot\sigma_{\mathrm{image}})$, where σ_{image}, the uncertainty in total counts for a single image, was assumed to follow Poisson statistics. This corresponds to an uncertainty of 0.032% using 5×10^6 count images that is in good agreement with the measured precision of 0.04% for the conventional method. The 0.04% precision for the conventional method and the 0.75% pass limit (as recommended by AAPM Report 52) implies a measured MSV pass limit, at the 95% confidence level, of $0.75\%+2\times 0.04\%=0.83\%$. The lower precision of the point-source method (0.145%) leads to a higher measured MSV pass limit of $0.75\%+2\times 0.145\%=1.03\%$, at the 95% confidence level.

The difference in precision may be partially attributed to the difference in counts per pixel for images acquired using the two methods. Compared to the average counts per pixel from a conventional (sheet source) 5×10^6 count image, approximately 35% of the pixels (or 700 out of 2000 pixels) in the point-source image have lower counts per pixel, and therefore those pixel values exhibit higher relative uncertainty. The lower counts per pixel observed in the point-source images occur at pixel locations away from the central axis due to inverse-square variation in photon flux for a near-field point source. A known feature of flat-field correction algorithms is that while they increase the value of low pixel counts, they also magnify the noise contribution from those pixels such that the image noise after flat-field correction is larger than the expected Poisson noise. The two additional corrections (Sec. II) applied to the raw point-source images may also contribute to the overall uncertainty in flat-field corrected total image counts. Therefore, the lower precision in MSV for the point-source method was not unexpected.

IV.C. Correlation between the MSV calculated with the two methods

The apparent lack of an obvious correlation between MSV calculated using the two methods using measured data from nine detectors does not appear unreasonable due to the narrow range of MSV measured and the fact that the measured population variance for each method was similar in magnitude to the precision of the MSV measurement. Therefore the observed scatter may predominantly arise due to random variations rather than lack of correlation between the methods. However, the inclusion of simulated data in the correlation analysis, which generated a larger range of MSV values, suggested a high degree of linear correlation between the two methods that was consistent with equivalence. The Bland-Altman plot of agreement in MSV between point-source and conventional methods suggested a possible bias of +0.12% for the point-source method. However, with a measured precision of 0.145% for the point-source method the magnitude of the bias is not statistically significant. The generation of large MSV values where images at a given view were acquired for different times, rather than just applying scale factors to a single image, proved difficult because the scan durations could not be set accurately enough to ensure matched pairs of simulated MSV values between conventional and point-source methods.

IV.D. Qualitative assessment of curvature-corrected images

Figure 4 demonstrates curvature correction of a near-field point-source image. The uncorrected raw image that displays substantial gradients or curvature across the image is shown in Fig. 4(a). The corresponding curvature-corrected image generated after fitting the image to the point-source image model (Appendix) is shown in Fig. 4(b). The peak count value in the point-source image was maintained in the curvature-corrected image as illustrated by the center profiles through the raw and the curvature-corrected images, see Fig. 4(c).

Small mechanical offsets in detector alignment and/or orientation with respect to the point source may offset the image peak location and/or create different fall-off gradients in different parts of the image depending on the tilt angle of the detector face with respect to the point source. Subtraction of counts between such offset images can result in gross artifact patterns that make visualization of subtle variations in detector uniformity or response an extremely difficult task. Figure 5 shows the difference images (0° image subtracted from the

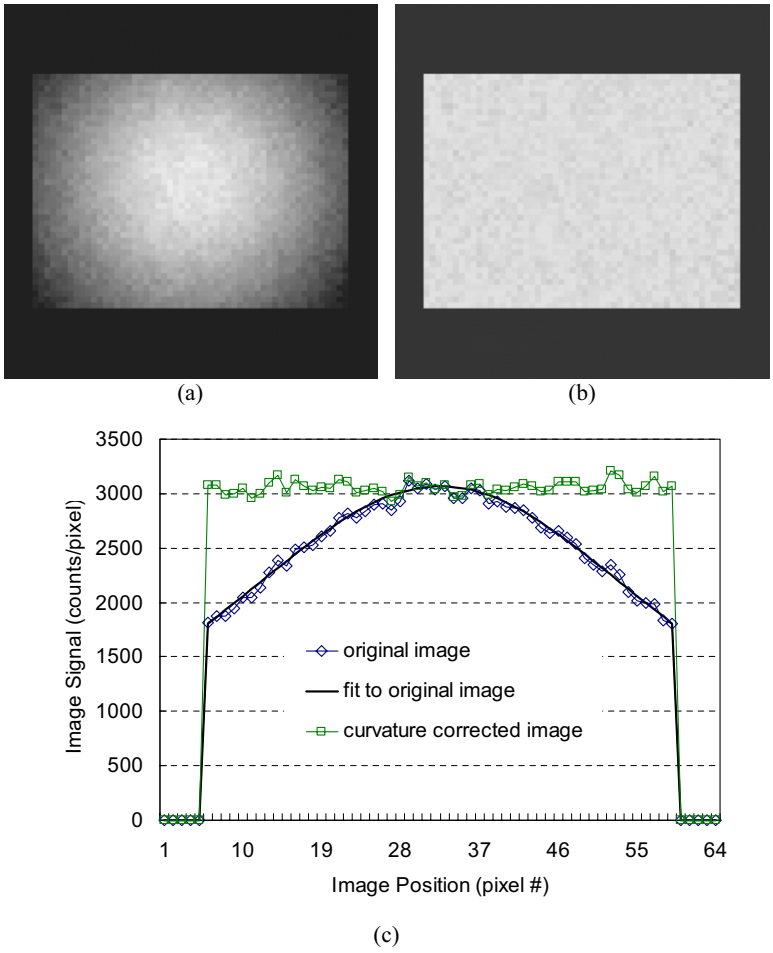

FIG. 4. A demonstration of the curvature-correction algorithm for a near-field point-source image as developed in the Appendix: (a) The uncorrected raw image, (b) the corresponding curvature-corrected image generated after fitting the image to the point-source image model, and (c) the center profiles through the raw and the curvature-corrected images.

90°, 180°, 270°, and 360° images) for two mechanically misaligned detectors using the point-source method. Figures 5(a) and 5(c) show the difference images for two different detectors where the original point-source images were not curvature corrected prior to subtraction, whereas Figs. 5(b) and 5(d) show the difference images where the original point-source images were curvature corrected prior to subtraction. Curvature correction of the point-source images prior to the generation of difference images largely removes the gross variations due to mechanical misalignment and renders the images more conducive to qualitative (visual) inspection for structured, nonrandom patterns representative of true variation in detector response as a function of gantry rotation angle (i.e., not due to the differences in the projection of a near-field point source onto detectors that may not have parallel faces). Note that neither detector has any real artifacts that should be seen.

IV.E. Advantages of the point-source method compared to the conventional method

Using a Co-57 sheet source with an activity of 300 MBq (~8 mCi) attached about 2.5 cm from the surface of the detector fitted with low-energy high-resolution collimators resulted in an acquisition time of about 8–10 min per image. The five images required per detector for MSV calculations thus amounts to approximately 40–50 min of data acquisition per detector. The total acquisition time, including attachment and removal of the sheet source, could take around 2 h for a dual-headed gamma camera. In contrast, using a Tc-99m point source with an activity of 90 kBq (~25 μCi) located near the gantry isocenter without collimation results in an acquisition time of about 2–3 min per image. The five images required per detector amount to approximately 10–15 min of data acquisition per detector. Since multiple detectors are acquired simultaneously with the proposed method, the total acquisition time for a dual-headed gamma camera, including initial setup of the point source, is only around 15–20 min.

One of the disadvantages of the point-source method, that is, however, not inherent to the methodology itself, is that tools and software programs for the postprocessing of the acquired images to correct for decay, distance, and, most importantly, curvature are not readily available on commercial gamma camera systems or processing computers. Another concern is that problems in the collimator, such as a loose core that shifts as a detector rotates, cannot be detected

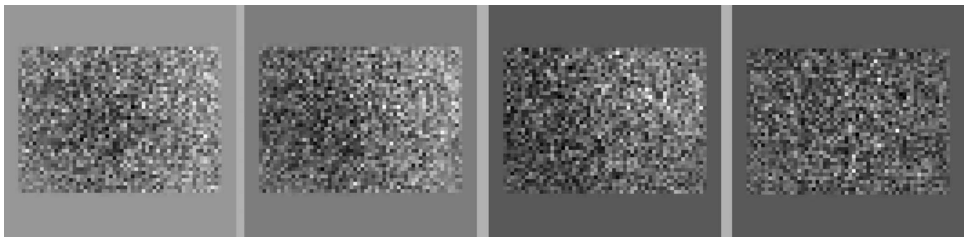

(a) Detector A: Curvature correction OFF

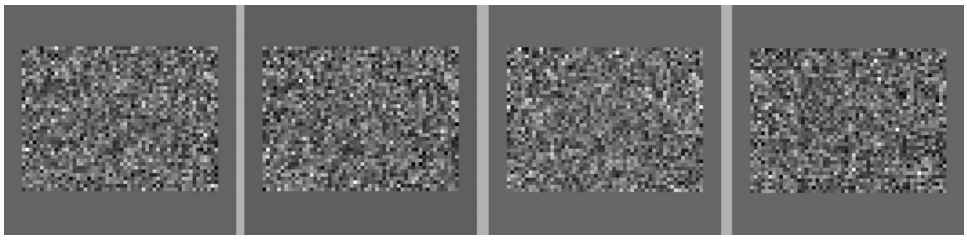

(b) Detector A: Curvature correction ON

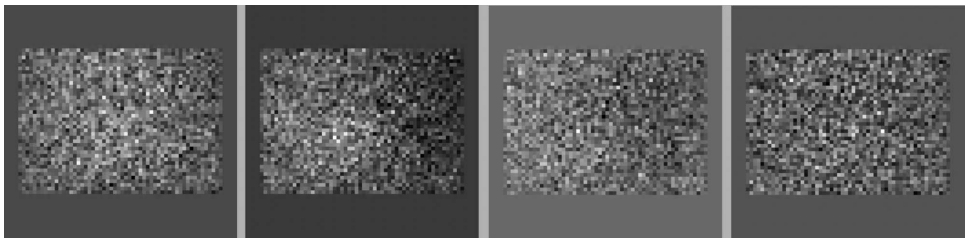

(c) Detector B: Curvature correction OFF

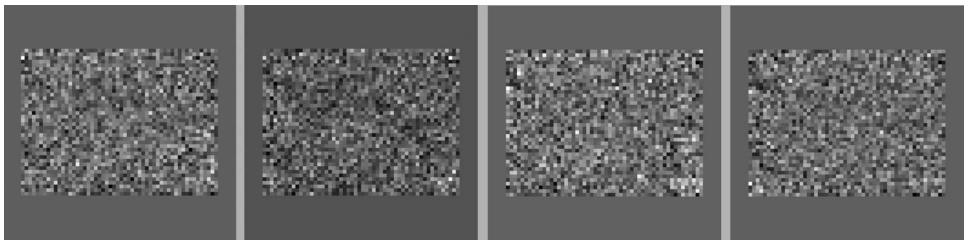

(d) Detector B: Curvature correction ON

FIG. 5. A demonstration of the use of curvature-corrected images for the qualitative inspection of structured, nonrandom patterns in subtracted images from two detectors. Note that neither detector has any real artifacts that should be seen. The differences (0° image subtracted from the 90°, 180°, 270°, and 360° images) for the point-source method are shown: [(a) and (c)] Without curvature correction prior to subtraction and [(b) and (d)] with curvature correction prior to subtraction.

by this new method. However, the authors' anecdotal experience is that when the system fails the MSV test, it is usually for intrinsic reasons, such as inadequate shielding from ambient magnetic fields.

V. CONCLUSION

In this work, an alternate methodology for evaluation of rotational uniformity and sensitivity variation for SPECT systems was successfully developed. This method acquires images concurrently on all detectors without collimation using a Tc-99m point source located near the isocenter. Prior to analysis, the intrinsic point-source images were corrected for (1) decay of Tc-99m between image acquisitions, (2) image curvature due to inverse-square variation in photon flux across the detector from a near-field point source and the effective thickness of the crystal at oblique angles of incidence, and (3) source-to-detector distance variation at different gantry positions since the point source is placed only approximately at the isocenter. Curvature correction was achieved by fitting each point-source image to an analytic function that was derived to describe the curvature in the signal intensity of the point-source image. Use of the curvature-correction fit to determine source-to-detector distance was validated. The MSV calculated using conventional and point-source methods exhibited a high degree of correlation and consistency with equivalence. The precision of the point-source method (0.145%) was lower than the conventional method (0.04%) but sufficient to test MSV. The AAPM Report 52 recommended MSV pass criterion, at the 95% confidence level, corresponds to $\leq$0.83% and $\leq$1.03% for the conventional and point-source methods, respectively. No statistically significant dependence of MSV with the point-

source method on the total image counts over a range of $(5-20)\times 10^6$ count was observed. Curvature correction of the images prior to the generation of difference images renders images more conducive to qualitative inspection for structured, nonrandom patterns. The major advantages of the new point-source method are as follows: (1) All detectors of a multiple detector gamma camera can be evaluated simultaneously, which substantially reduces the time required for rotational uniformity testing, (2) MSV estimates are insensitive to exact setup since the analytic fit of the image accounts for the distance and the noncentered source placement, and (3) there is reduced risk of accidental damage to the collimators and patient proximity detection system.

APPENDIX: DERIVATION OF THE POINT-SOURCE IMAGE MODEL

The photon flux from a point source incident on a detector follows the distribution of solid angle subtended by the detector. The solid angle Ω subtended by a surface S is defined as the area of the surface's projection onto a unit sphere. In general, the solid angle can be written as

$$\Omega = \int\int_s d\Omega = \int\int_s \frac{\hat{n}\cdot d\vec{a}}{r^2}, \tag{A1}$$

where $\hat{n}$ is a unit vector from the origin, $d\vec{a}$ is the differential area of surface S, and r is the distance from the origin to the location of $d\vec{a}$. To explicitly compute the point-source image function, consider the distribution of solid angle $d\Omega$ subtended by a rectangle at distance D and centered on the origin. The solid angle $d\Omega$ can be rewritten in Cartesian coordinates using

$$\hat{n}\cdot d\vec{a} = \cos(\theta)\cdot dx\cdot dy \quad \text{and} \quad r^2 = x^2+y^2+D^2, \tag{A2}$$

where

$$\cos(\theta) = \frac{D}{r} = \frac{D}{\sqrt{x^2+y^2+D^2}}.$$

Substitution of Eq. (A2) in Eq. (A1) yields

$$d\Omega = \frac{D\cdot dx\cdot dy}{(x^2+y^2+D^2)^{3/2}}. \tag{A3}$$

Therefore, the distribution of solid angle (f_Ω) subtended by the detector at distance D with the point source P projecting onto the detector plane at location (x_0,y_0), as shown in Fig. 6, is given by

$$f_\Omega = \frac{D}{((x-x_0)^2+(y-y_0)^2+D^2)^{3/2}} \propto \frac{1}{D^2}. \tag{A4}$$

The function f_Ω describes the photon fluence incident on the detector surface. We next account for the different path lengths, and therefore variable photon absorption, through the scintillator for photons at oblique angles. If d is the path length of photon through the scintillator intersecting at $R(x,y)$ and T is the thickness of the scintillator, then using properties of similar triangles between POR and $RO'R'$ (see Fig. 6), we get $PR/PO=RR'/RO'$. But $PO=D$, $RR'=d$, $RO'=T$, and $PR^2=PO^2+OR^2=D^2+(x-x_0)^2+(y-y_0)^2$, yielding

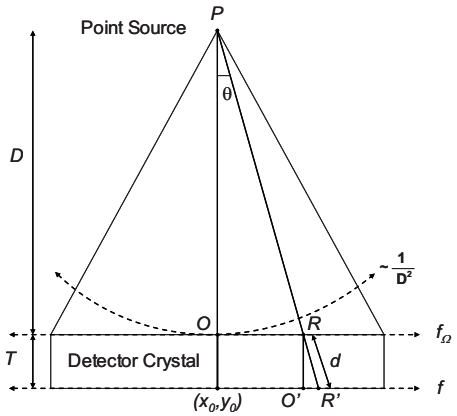

FIG. 6. A schematic of the point-source imaging geometry for the proposed point-source methodology for testing rotational uniformity and sensitivity variations. Distances and variables shown are discussed at depth in the Appendix. The distances are not shown to scale but adjusted for clarity (e.g., $D \gg T$).

$$d = T\cdot\left(1+\frac{(x-x_0)^2+(y-y_0)^2}{D^2}\right)^{1/2}. \tag{A5}$$

The photon fluence f measured by the detector can be expressed by combining Eqs. (A4) and (A5) as

$$f = N\cdot\left[\frac{1-e^{-\mu d}}{1-e^{-\mu T}}\right]\cdot\left\{\frac{D}{((x-x_0)^2+(y-y_0)^2+D^2)^{3/2}}\right\}, \tag{A6}$$

where the differential transmission across the detector due to photon attenuation by the scintillator is given by the term in the square bracket and N is a normalization scalar related to the source activity.

[a]Author to whom correspondence should be addressed. Electronic mail: skappadath@mdanderson.org; Telephone: 713-745-2835; Fax: 713-563-8842.

[1]National Electrical Manufacturers Association (NEMA) Standards Publication No. NU 1-1994, "Performance measurements of scintillation cameras" (NEMA, Washington, DC, 1994). www.nema.org.
[2]American Association of Physicists in Medicine (AAPM) Report No. 22, "Rotating scintillation camera SPECT acceptance testing and quality control" (AAPM, College Park, MD, 1987). www.aapm.org.
[3]L. S. Graham, F. H. Fahey, M. T. Madsen, A. van Aswegen, and M. V. Yester, "Report of SPECT performance: Report of Task Group 4, Nuclear Medicine Committee," Med. Phys. **22**(4), 401–409 (1995).
[4]C. I. Coleman, "Effects of perturbing magnetic fields on the performance of photoelectronic sensors," Rev. Sci. Instrum. **53**, 735–739 (1982).
[5]T. K. Johnson and D. L. Kirch, in *Emission Computed Tomography: Current Trends*, edited by P. D. Esser (The Society of Nuclear Medicine, New York, 1983).
[6]N. R. Ullman, *Statistics: An applied approach* (Xerox College Publishing, 1972).
[7]W. H. Press, B. P. Flannery, S. A. Teukolsky, and W. T. Vetterling, *Numerical Recipes in C* (Cambridge University Press, New York, 1988).
[8]J. M. Bland and D. G. Altman, "Statistical methods for assessing agreement between two methods of clinical measurement," Lancet **1**(8476), 307–310 (1987).
[9]B. A. Rosner, *Fundamentals of Biostatistics*, 6th ed. (Brooks-Cole, Belmont, 2006).